Solar Phys (2019) 294:123
https://doi.org/10.1007/s11207-019-1514-7

Global Solar Magnetic Field and Interplanetary Scintillations During the Past Four Solar Cycles

K. Sasikumar Raja[1,2] · P. Janardhan[1] · Susanta Kumar Bisoi[3] · Madhusudan Ingale[4] · Prasad Subramanian[4] · K. Fujiki[5] · Milan Maksimovic[2]

Received: 25 April 2019 / Accepted: 23 August 2019

Abstract The extended minimum of Solar Cycle 23, the extremely quiet solar-wind conditions prevailing and the mini-maximum of Solar Cycle 24 drew global attention and many authors have since attempted to predict the amplitude of the upcoming Solar Cycle 25, which is predicted to be the third successive weak cycle; it is a unique opportunity to probe the Sun during such quiet periods. Earlier work has established a steady decline, over two decades, in solar photospheric fields at latitudes above 45° and a similar decline in solar-wind microturbulence levels as measured by interplanetary scintillation (IPS) observations. However, the relation between the photospheric magnetic fields and those in the low corona/solar-wind are not straightforward. Therefore, in the present article, we have used potential-field

✉ K. Sasikumar Raja
sasikumar-raja.kantepalli@obspm.fr; sasikumarraja@gmail.com

P. Janardhan
jerry@prl.res.in

S.K. Bisoi
susanta@nao.cas.cn

M. Ingale
31mayur83@gmail.com

P. Subramanian
p.subramanian@iiserpune.ac.in

K. Fujiki
fujiki@isee.nagoya-u.ac.jp

M. Maksimovic
milan.maksimovic@obspm.fr

1 Physical Research Laboratory, Navrangpura, Ahmedabad 380 009, India

2 LESIA, Observatoire de Paris, Université PSL, CNRS, Sorbonne Université, Université de Paris, 5 place Jules Janssen, 92195 Meudon, France

3 Key Laboratory of Solar Activity, National Astronomical Observatories, Chinese Academy of Sciences, Beijing 100 012, People's Republic of China

4 Indian Institute of Science Education and Research, Pashan, Pune 411 008, India

5 Institute for Space–Earth Environmental Research, Nagoya, Japan

Published online: 16 September 2019

source-surface (PFSS) extrapolations to deduce global magnetic fields using synoptic magnetograms observed with National Solar Observatory (NSO), Kitt Peak, USA (NSO/KP) and *Solar Optical Long-term Investigation of the Sun* (NSO/SOLIS) instruments during 1975 – 2018. Furthermore, we have measured the normalized scintillation index [m] using the IPS observations carried out at the Institute of Space–Earth Environment Research (ISEE), Japan during 1983 – 2017. From these observations, we have found that, since the mid-1990s, the magnetic field over different latitudes at 2.5 $R_\odot$ and 10 $R_\odot$ (extrapolated using the PFSS method) has decreased by $\approx 11.3 - 22.2\%$. In phase with the declining magnetic fields, the quantity m also declined by $\approx 23.6\%$. These observations emphasize the inter-relationship among the global magnetic field and various turbulence parameters in the solar corona and solar-wind.

Keywords Magnetic fields, photosphere · Magnetic fields, corona · Magnetic fields, models · Sunspots, magnetic fields

1. Introduction

The magnetic field plays a crucial role in understanding the various phenomenon that occur on the Sun and in the solar atmosphere. Most of the features (*e.g.* sunspots, filaments, prominences, coronal holes) and transient events (*e.g.* solar flares, coronal mass ejections, and non-thermal radio bursts) are related to the magnetic field. Recent work has established a steady decline, over the past two decades, in solar photospheric magnetic fields at latitudes above 45° and a similar decline in solar-wind micro-turbulence levels as measured by interplanetary scintillation (IPS) observations (Janardhan, Bisoi, and Gosain, 2010; Janardhan *et al.*, 2011, 2015). Solar Cycle 24 has also shown a significant asymmetry in the times of reversals of the polar field in the two solar hemispheres (Janardhan *et al.*, 2018), leading to speculation as to whether we are heading toward another Grand solar minimum like the Maunder minimum if the decline in the photospheric fields will continue beyond 2020, the expected minimum of the current Solar Cycle 24.

Although photospheric magnetic fields are available for many decades (see for example Hale, 1908), our understanding of the coronal magnetic fields is limited (Lin, Penn, and Tomczyk, 2000). Direct methods such as the Zeeman effect (Harvey, 1969) and the Hanle effect (Mickey, 1973; Querfeld and Smartt, 1984; Arnaud and Newkirk, 1987) fail in the low-density corona. Magnetic-field measurements in the outer corona derived using Faraday-rotation observations are limited due to various (observational and instrumental) constraints (Stelzried *et al.*, 1970; Bird, 1981, 1982). Magnetic-field measurements that are reported using a few indirect techniques using polarization observations of solar radio bursts (Sastry, 2009; Ramesh, Kathiravan, and Sastry, 2010; Sasikumar Raja and Ramesh, 2013; Sasikumar Raja *et al.*, 2014) are rare. Therefore, in the inner corona, magnetic-field measurements are limited to extrapolation techniques (Schatten, Wilcox, and Ness, 1969; Schrijver and Title, 2003).

In this article, we use the photospheric synoptic magnetogram data observed using National Solar Observatory (NSO), Kitt Peak, USA (NSO/KP) and *Solar Optical Long-term Investigation of the Sun* (NSO/SOLIS) instruments. We used potential-field source-surface (PFSS) extrapolation routines available in the IDL/solarsoft library (Freeland and Handy, 1998) to extrapolate the magnetic fields to 2.5 and 10 $R_\odot$ (Altschuler and Newkirk, 1969; Schatten, Wilcox, and Ness, 1969; Hoeksema, 1984; Wang and Sheeley, 1992; Schrijver and

De Rosa, 2003) to examine if the extended decline in the photospheric fields (maybe high-latitude photospheric fields?) is mirrored in the coronal fields as well. The magnetogram data that we used were observed during 1975 – April 2018. On the other hand, we used the observations of interplanetary scintillation (IPS) carried out at the Institute for Space–Earth Environmental Research (ISEE), Japan during 1983 – 2017. Using the IPS observations of 27 radio sources carried out in the heliocentric distance 0.2 – 0.8 AU (astronomical unit, 1 AU = 215 $R_{\odot}$), we measured the normalized scintillation index [m]. In this article, we examine the relation between the global magnetic fields (at the photospheric level and in the inner solar-wind) and the level of interplanetary scintillations (characterized by m).

The observational details of magnetograms and interplanetary scintillations are discussed in Section 2. The PFSS extrapolation technique, measurements of magnetic fields over different latitudes, and the normalized scintillation index [m] are discussed in Section 3. The observational results and discussions are described in Section 4. The summary and conclusions are given in Section 5.

2. Observations

The observational details of the magnetogram data, IPS observations, and sunspot number are discussed in this section.

2.1. Magnetogram Data

In the present study, we use the synoptic magnetograms from NSO/KP observed during 1975.13 – 2003.66. This corresponds to the Carrington Rotations (CR) CR 1625 to CR 2006. Since 2003.66, such observations are carried out using the *Vector Stokes Magnetograph*, one of the three instruments that comprise SOLIS. From CR 2007 to CR 2206, we used the data observed using the SOLIS instrument. The synoptic maps are prepared using the full-disk magnetograms (see Figure 1) observed over a Carrington rotation. The synoptic maps were stored in the FITS format. The data are stored as a 180 × 360 array format. This means that the resolution of a synoptic map is 1° in both longitudinal (0° – 360°) and latitudinal (−90° to 90°) directions. The full-disk magnetograms are mapped into longitude and latitude coordinates and added together to form the final synoptic magnetogram (see upper panel of Figure 2).

2.2. Interplanetary Scintillation Data

Inter-planetary scintillation (IPS) or intensity scintillation is a well-established technique to probe the solar wind in the inner heliosphere. IPS is basically a diffraction phenomenon in which coherent electromagnetic radiation from a distance radio source experiences scattering when it is observed through the turbulent and refracting solar wind and thus causes temporal variation of the flux density when observed from Earth (Hewish, Scott, and Wills, 1964; Ananthakrishnan, Coles, and Kaufman, 1980; Kojima and Kakinuma, 1990; Janardhan and Alurkar, 1993; Janardhan *et al.*, 1996; Asai *et al.*, 1998; Manoharan, 2010; Tokumaru, Kojima, and Fujiki, 2010).

ISEE has been carrying out IPS observations using a three-station facility located at Fuji (long. 138°36′42″ E, lat. 35°25′36″ N), Toyokawa (long. 137°22′09″ E, lat. 34°50′05″ N), Sugadaira (long. 138°19′16″ E, lat. 36°31′12″ N) during 1983 – 1994. In addition, a fourth station has been commissioned at Kiso (long. 137°37′49″ E, lat. 35°47′34″ N) in 1994 and

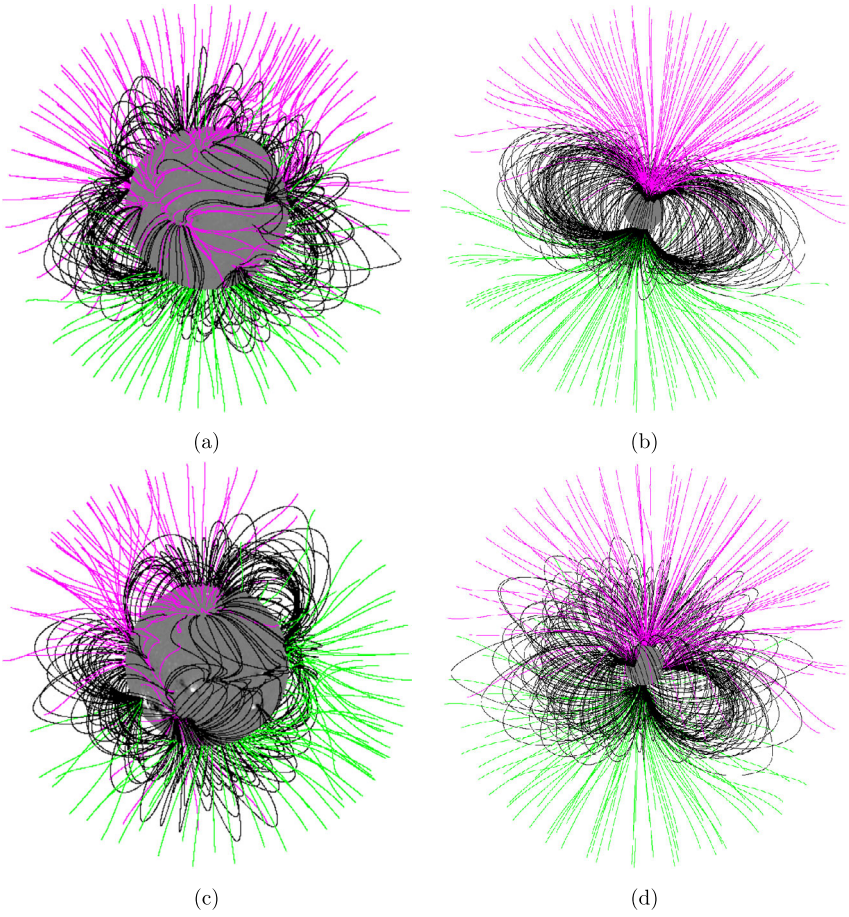

Figure 1 The *upper* (**a** and **b**) and *lower* (**c** and **d**) panels represents the PFSS extrapolated magnetic fields derived from the full-disk magnetograms observed on 9 August 2011 (solar minimum) and 18 July 2004 (solar maximum), respectively. The *left* (**a** and **c**) and *right* (**b** and **d**) panels show the extrapolated magnetic fields from 1.5 – 2.5 $R_\odot$ and 5 – 10 $R_\odot$, respectively. The *gray colored disk* at the center is the magnetogram observed at the NSO/KP or NSO/SOLIS instruments. The *black lines* represent the closed field lines. The lines, respectively, in *magenta and green* indicate the negative and positive polarities of the open magnetic–field lines.

then onwards a four-station facility has been used to measure the solar-wind speed by using cross-correlation analysis. The current four-station network provide more robust estimates of the solar-wind speed owing to the redundancy in the baseline geometry. However, the scintillation index was measured using the telescope located at Fuji during 1983 – 1994. After 1994, a new facility located at Kiso has been used to measure the scintillation index. We note here that the telescopes located at all four stations are identical.

2.3. Sunspot Number

In this work, we make use of the revised sunspot numbers (ver-2.0) (www.sidc.be/silso/newdataset) prepared by re-calibrating the sunspots that were observed over 400 years (Clette *et al.*, 2015).

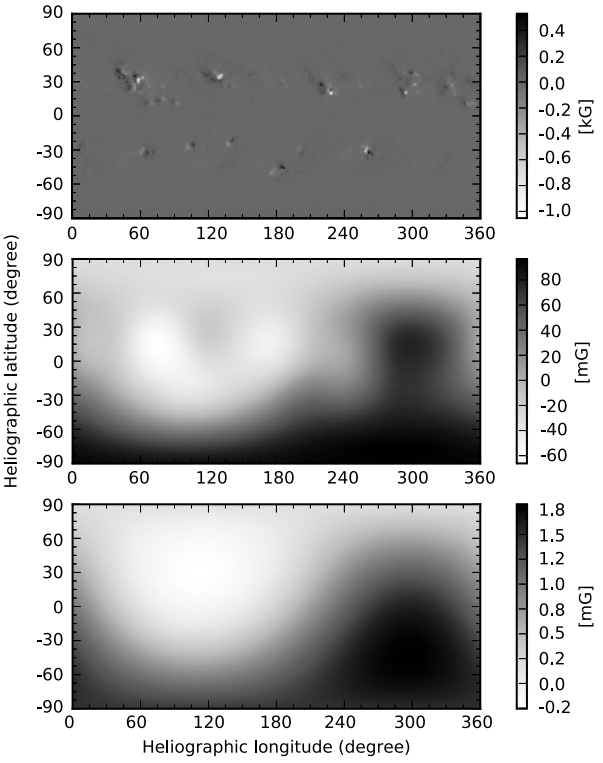

Figure 2 The synoptic magnetogram (*upper panel*) was observed during the CR 2114 using the NSO/SOLIS instrument at the wavelength 630.150 nm. The *upper panel* shows the distribution of observed photospheric magnetic fields. The *middle* and *lower panels* are the extrapolated synoptic magnetograms (of the one in the *upper panel*) to 2.5 and 10 $R_{\odot}$, respectively.

3. Data Analysis

In this section we describe the PFSS extrapolation technique and the way that we measured the averaged magnetic fields over different latitude regions using the synoptic magnetogram data (see Sections 3.1 and 3.2). In addition, we discuss the way that we measured the normalized scintillation index using the IPS observations (see Section 3.3).

3.1. PFSS Extrapolation

The photospheric magnetic field and its spatial distribution are routinely observed using magnetographs. However, coronal magnetic fields are challenging to probe owing to the low coronal density, as previously mentioned. Therefore, global magnetic fields in the corona are commonly modeled using the potential-field source-surface (PFSS) model (Schatten, Wilcox, and Ness, 1969). The upper (a and b) and lower (c and d) panels of Figure 1 show the so-called "hairy Sun" images observed on 9 August 2011 (during solar minimum) and 2004 July 18 (during solar maximum), respectively. Similarly the left (a and c) and right (b and d) panels represents the extrapolated field lines drawn from 1.5 – 2.5 $R_{\odot}$ and from 5 – 10 $R_{\odot}$, respectively, using the PFSS model. The field lines in black are closed, *i.e.* they intersect the inner boundary (*i.e.* the photosphere) in two places. The field lines in magenta and green colors are open, *i.e.* they intersect both inner and outer boundaries (the source surface) of the model. The magenta and green colors indicate the negative or positive polarities, respectively (www.lmsal.com/~derosa/pfsspack/).

In the present work, we used the synoptic magnetograms observed at NSO/KP and NSO/SOLIS instruments and extrapolated the magnetic field to 2.5 and 10 $R_\odot$ using the PFSS model. The key assumption of this model is that there is zero electric current in the solar corona. Usually this method is applied up to the heliocentric distance 2.5 $R_\odot$. Beyond this distance, in general, the magnetic fields are radial and therefore, we extrapolated further to 10 $R_\odot$. The upper panel of Figure 2 shows the observationally derived synoptic magnetogram at the photospheric height. The middle and lower panels are the extrapolated magnetograms to the heliocentric distances 2.5 and 10 $R_\odot$. Note that we used this model because it is one of the basic and routinely used models when compared to other models such as the current-sheet source-surface (CSSS) model (Zhao and Hoeksema, 1995) and non-linear force-free models (van Ballegooijen, Priest, and Mackay, 2000; Mackay and van Ballegooijen, 2006).

3.2. Magnetic-Field Measurements

Using the magnetograms observed at photospheric height and the extrapolated magnetograms at 2.5 and 10 $R_\odot$, we have studied the magnetic-field variations over different ranges of latitudes. As we are interested in latitudinal variation of the magnetic field, we find an averaged magnetic field along longitudes $[\phi_{i,n}]$ using

$$\phi_{i,n} = \frac{\Sigma_{j=1}^{360}\, \phi_{i,j,n}}{360}, \tag{1}$$

where i, j and n are the latitude, longitude, and CR number. After the average, the size of the array reduces to 180×1. Then we measured the averaged magnetic field $[\phi_n]$ over selected latitude intervals for a given CR number $[n]$ using

$$\phi_n = \frac{\Sigma_{i=k}^{p}\phi_{i,n}}{p-k+1}, \tag{2}$$

where k and p are the row numbers corresponding to the selected latitude bin. Using Equations 1 and 2, we have measured the magnetic field over different latitude regions of the Sun and solar corona: i) equatorial or toroidal field (*i.e.* the fields ranging in the latitude regions from $0^\circ - 45^\circ$); ii) Mid-latitude fields (*i.e.* the fields ranging in the latitude regions from $46^\circ - 78^\circ$; iii) the fields ranging from $0^\circ - 78^\circ$ (henceforth referred to as Region A fields); and iv) the polar or polar cap fields (*i.e.* the fields ranging in the latitude region from $78^\circ - 90^\circ$). The averaged magnetic fields measured over these latitude regions are shown in Figures 3 and 4.

3.3. Interplanetary Scintillations

If there is an enhancement or depletion of density fluctuations in the solar-wind along the line-of-sight (LOS) to the observed radio source, then there is a corresponding change in scintillation index $[m]$, defined as

$$m = \frac{\Delta S}{\langle S \rangle}, \tag{3}$$

where ΔS and $\langle S \rangle$ are the scintillation flux and the mean source flux, respectively. The quantity ΔS is computed from the power spectrum $[P(f)]$ of the IPS observation using

$$\Delta S = \int_0^\infty P(f)\, \mathrm{d}f. \tag{4}$$

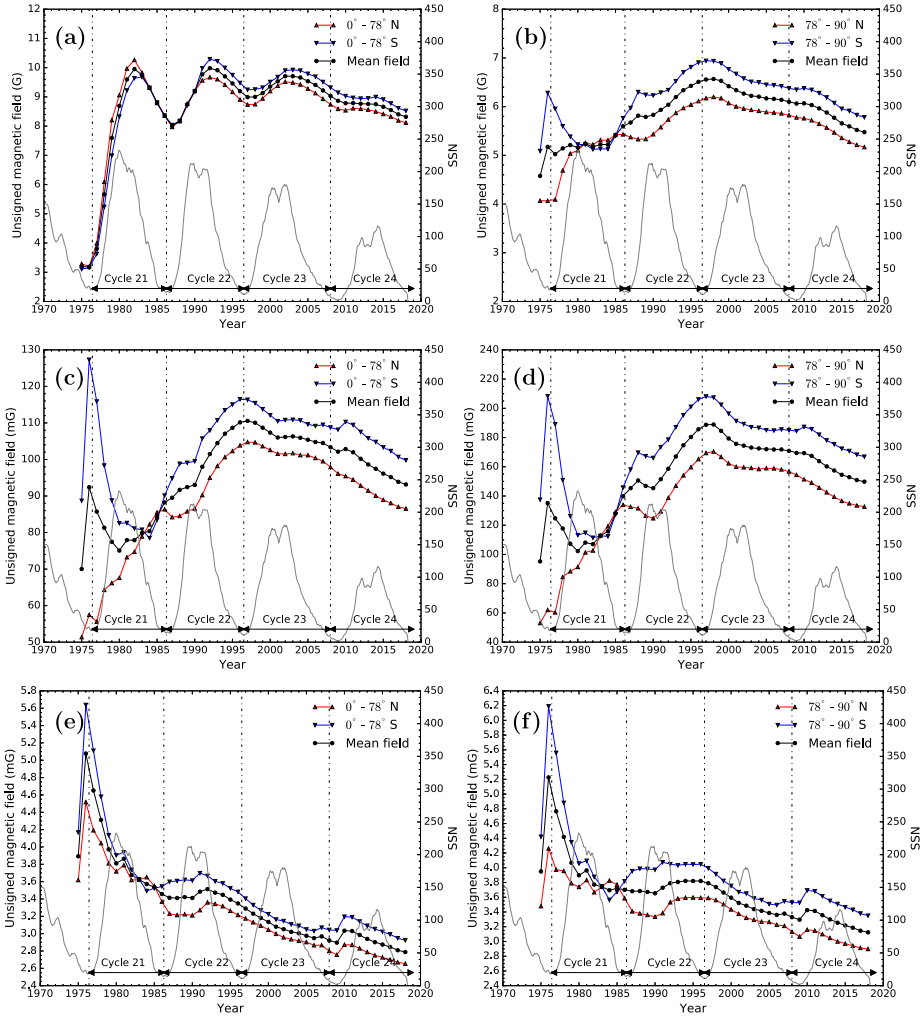

Figure 3 Variation of magnetic field with the solar cycle. The *left* (**a**, **c**, **e**) and *right* columns (**b**, **d**, **f**) show the average of Region A and poloidal fields, respectively. *In each panel* the *triangles pointing upward and triangles pointing downward* indicate the northern and southern hemispheric fields. The *circle in black* indicate the average of both northern and southern hemispheric fields. The *gray solid line* shows the monthly averaged sunspot number (SSN). Panels **a** and **b** shows the field on photosphere. The panels **c** and **d** show the extrapolated field at 2.5 $R_\odot$. Panels **e** and **f** show the extrapolated field at 10 $R_\odot$.

The mean source flux [$\langle S \rangle$] can be measured by averaging the difference between on-source and off-source fluxes (Tokumaru, Kojima, and Fujiki, 2010). IPS observations of 215 compact extragalactic and radio sources have been carried out on regular basis at 327 MHz. We should note here that all of these sources have a finite angular diameter ranging from ≈ 10 to 500 milliarcsecond (mas) and observed over different heliocentric distances range from 0.2 to 0.8 AU. It was found that, in general, the quantity m increases with the decreasing heliocentric distance up to a certain distance called turn-over distance and inside this distance it decreases rapidly with the further decrement in the distance. On the other hand, m decreases

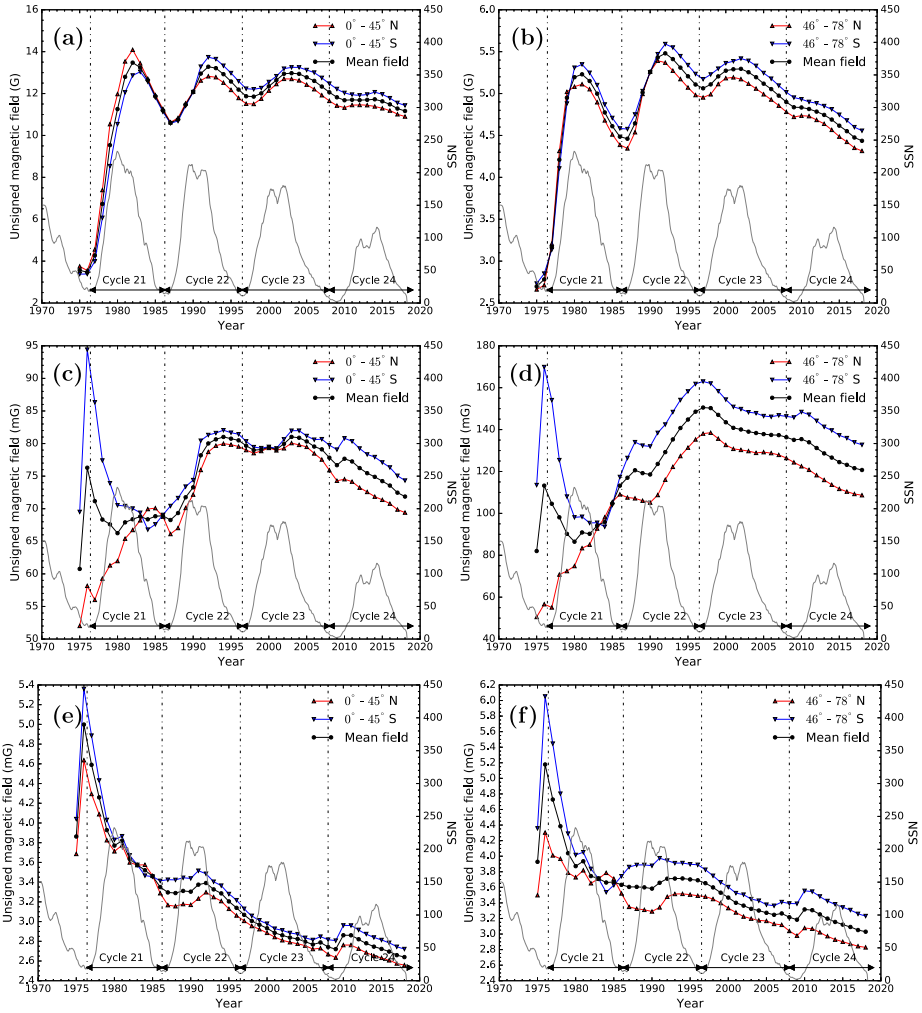

Figure 4 Variation of magnetic field with the solar cycle. The *left* (**a**, **c**, **e**) and *right columns* (**b**, **d**, **f**) show the toroidal and mid-latitude fields, respectively. *In each panel* the *triangles pointing upward and triangles pointing downward* indicate the northern and southern hemispheric fields. The *circles in black* indicate the average of both northern and southern hemispheric fields. The *gray solid line* shows the monthly averaged sunspot number (SSN). Panels **a** and **b** shows the field on the photosphere. The Panels **c** and **d** show the extrapolated field at 2.5 $R_{\odot}$. Panels **e** and **f** show the extrapolated field at 10 $R_{\odot}$.

if the angular size of the radio source increases. Also, for an ideal point source the scintillating flux will be equal to the mean source flux and thus the scintillation index will be equal to unity at a certain distance (*e.g.* at 327 MHz, the distance at which $m = 1$ corresponds to 0.2 AU) and then decreases with the further increment in the heliocentric distance. Therefore, following Janardhan *et al.* (2011) and Bisoi *et al.* (2014), we have normalized the m so that it is independent of the heliocentric distance and a finite source size at that distance. We make a note that Janardhan *et al.* (2011) have reported the m after elimination of dependence of the heliocentric distance but not corrected for the finite source sizes. In Bisoi

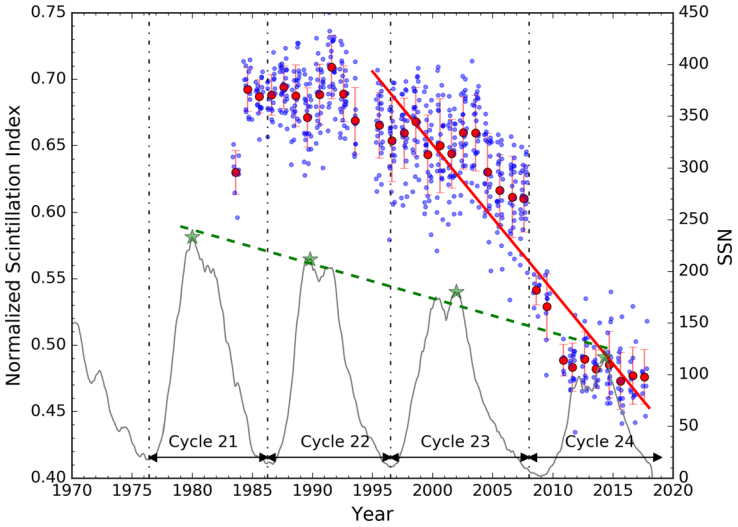

Figure 5 Variation of the normalized scintillation index [m] over different years is shown. The *blue circles* indicate the annually averaged m for different sources. The *red circles* indicate the annual average of all sources observed in that year. The *fit to the red circles* (*red solid curve*) explicitly shows that the quantity m has been declining since $\approx$1995. These observations are carried out using the facility at ISEE, Japan at 327 MHz during 1983 – 2017. The *gray curve* indicate the sunspot number observed during this period. The *dashed green line* is a fit to observed highest sunspot number during solar maximum (indicated using *green stars*) also shows the declining highest sunspot number since Solar Cycle 21.

et al. (2014), the reported m is corrected for both dependence of heliocentric distance and the finite source sizes.

For the sake of completeness we have summarized the method of normalization adopted in this article: i) In order to remove the heliocentric-distance dependence of m, each observation of m has to be normalized by that of a point source at that distance. We know that the source 1148-001 has the smaller angular diameter of $\lesssim$10 mas at 327 MHz and therefore we treat that source to be an ideal point source (Venugopal *et al.*, 1985). ii) Similarly, we have eliminated the dependence of finite source sizes using a least-square minimization to determine which of the curves best fits the data for a given source (see Marians, 1975; Bisoi *et al.*, 2014). Assuming the radio source 1148-001 as a point source, the observed values of m of all other sources were multiplied by a factor equal to the difference between the best-fit Marians curve for the given source and the best-fit Marians curve for 1148-001 at the corresponding heliocentric distance (Bisoi *et al.*, 2014). Therefore, all measurements of m reported in this article were independent of a distance and the sources sizes.

After normalization, we have selected the sources that have at least 400 observations (during 1983 – 2017) and are uniformly distributed over the entire heliocentric distance (*i.e.* 0.2 – 0.8 AU) without significant data gaps. After such a rigorous filtering, we were left with 27 sources (out of the 215 regularly observed sources), which cover right ascensions over 24 hours and a wide range of declinations. The blue circles in Figure 5 indicate the measured annual average of m that corresponds to the 27 sources separately. The red circles indicate the annual average of m for all 27 sources in a given year. We would like to make note that in order to avoid unusual error bars (during Solar Cycle 24) because of the significant drop in m after 2008, we have measured the error bars separately for the years 1983 – 2008 and

2009 – 2017. The 1σ error bars of the annually averaged m values of the observed sources in that year are shown in Figure 5.

4. Results and Discussion

Recent reports using angular-broadening observations show that various turbulent parameters (*e.g.* amplitude of turbulence, density-modulation index) correlate well with the solar cycle (Bisoi *et al.*, 2014; Sasikumar Raja *et al.*, 2016, 2017). In this article, we attempted to explore the relationship between the global magnetic-field strength and the turbulence parameters. As previously mentioned, there is no direct method to measure the magnetic-field strength in the corona and hence in order to have some idea of the magnetic-field strength at 10 $R_\odot$ (the distance where, at present, we can probe the solar-wind using IPS observations), we used the PFSS extrapolation technique. We opt for this technique because it is basic and widely used in recent times. This technique works well to heliocentric distances up to 2.5 $R_\odot$. However, as the global magnetic-field lines are radial beyond this height, we extrapolated further to 10 $R_\odot$. As discussed in Section 3, we inspected the magnetic field at photosphere, 2.5, and 10 $R_\odot$ over different latitudes.

Figures 3 and 4 show the variation of the global magnetic field with the solar cycle. In Figure 3 panels a, c, e and panels b, d, f show the average of Region A (latitudes $0^\circ - 78^\circ$) and polar or poloidal fields. Similarly, in Figure 4, panels a, c, e and panels b, d, f show the average of the field in equatorial or toroidal and mid-latitude fields, respectively. In both Figures 3 and 4, in each panel the triangles pointing upward and triangles pointing downward indicate the northern and southern hemispheric fields. The circles in black indicate the mean field of both northern and southern hemispheric fields (*i.e.* average of the points shown in triangles both upward and downward). In each panel, for reference, the smoothed, monthly average sunspot number (SSN) is shown as a gray solid line (www.sidc.be/silso/DATA/SN_ms_tot_V2.0.txt). In both Figures 3 and 4, panels a and b show the magnetic field at photospheric heights. Panels c and d show the extrapolated field at 2.5 $R_\odot$ and panels e and f show the extrapolated field at 10 $R_\odot$.

From Figures 3 and 4, it is clear that the magnetic field has been declining since the mid-1990s. Various observationally derived parameters are tabulated in Table 1. The latitude range over which the magnetic field is averaged is shown in column 2. The year of the beginning of significant decline of the field is shown in column 3 and the corresponding field in column 4. Similarly for the year 2018 the measured magnetic field is shown in column 6. We measured the decrement in magnetic field (in percent) from the mid-1990s to 2018 (at photosphere, 2.5, and 10 $R_\odot$) and tabulated it in column 7. We found that the magnetic fields over different range of latitudes and heliocentric distances declined by 11 – 22.2%. These results are very significant support for the conclusion that not only were the polar fields declining since mid-1990, as previously reported (Janardhan *et al.*, 2011, 2015) but the overall (global) coronal magnetic field is also declining. We found that, in phase with the global magnetic fields, the quantity m also declined by 23.6% from the mid-1990s to 2017. These results show that the global magnetic field is controlling the turbulence characteristics in the solar corona and solar-wind.

Another notable observation is that we see a variation of the magnetic field at the photospheric height in correlation with the sunspot number (see panels a and b of Figures 3 and 4). We examined such variation (from solar maximum to minimum) of the mean magnetic field (see Figures 3 and 4) in each solar cycle (from Solar Cycle 22 to 24) and found that it varied

Table 1 The averaged magnetic-field strength at different epochs (mid-1990s and 2018) over different latitudes are shown. The decrement of the magnetic field [%] over these epochs are shown in *column 7*. The measurements are tabulated for photospheric height, 2.5, and 10 $R_\odot$.

No.	Latitude range	Epoch – I		Epoch – II		Decrement [%]
		Year	Mean field [G]	Year	Mean field [G]	
(1)	(2)	(3)	(4)	(5)	(6)	(7)
Photosphere						
1	0° – 78°	1992	9.98	2018	8.32	16.6
2	78° – 90°	1997	6.56	2018	5.48	16.5
3	0° – 45°	1992	13.28	2018	11.17	15.9
4	45° – 78°	1992	5.48	2018	4.44	19.1
2.5 $R_\odot$						
1	0° – 78°	1996	0.11	2018	0.09	15.4
2	78° – 90°	1997	0.19	2018	0.15	20.6
3	0° – 45°	1994	0.08	2018	0.07	11.3
4	45° – 78°	1997	0.15	2018	0.12	19.8
10 $R_\odot$						
1	0° – 78°	1992	3.51×10^{-3}	2018	2.79×10^{-3}	20.6
2	78° – 90°	1994	3.82×10^{-3}	2018	3.12×10^{-3}	18.2
3	0° – 45°	1992	3.39×10^{-3}	2018	2.64×10^{-3}	22.2
4	45° – 78°	1993	3.71×10^{-3}	2018	3.03×10^{-3}	18.4

by $\approx 5-10\%$. We found that such oscillating behavior (due to sunspots) disappears in the solar corona and solar wind (see panels c, d, e and f of Figures 3 and 4) and shows a clear monotonic decline of the coronal magnetic field (by $11-22.2\%$).

We also would like to make a note that in Figure 5, the quantity m (the red circles) shows a negative jump near the solar maximum which can be interpreted as follows: Sasikumar Raja *et al.* (2016) have reported that the density modulation index (*i.e.* $\epsilon_N = \Delta N/N$; where ΔN and N are the density fluctuations and the background density, respectively) positively correlates with the solar-wind speed. For the sake of completeness we provide the explanation given by them as follows. It was reported that the ϵ_N positively correlates with the temperature of solar-wind protons (Celnikier, Muschietti, and Goldman, 1987). Also, it was found that at 1 AU, the proton temperature positively correlates with solar-wind speed (Lopez and Freeman, 1986). Taken together, authors have concluded that ϵ_N should be larger in the fast solar-wind and lower in the slow solar-wind. We also know that during solar minimum the global magnetic field is dipolar and therefore, during solar minimum higher latitudes drive the fast solar-wind (because of the dominant polar coronal holes) and drive the slow solar wind near the low latitudes. On the other hand, during solar maximum, the global magnetic field is multi-polar and thus drives the slow solar wind in all helio-latitudes as the polar coronal holes are not prevalent (Asai *et al.*, 1998; McComas *et al.*, 2000). Therefore, during solar maximum the slow solar wind suggests the lower density modulation index, which in-turn is proportional to the quantity m (see Bisoi *et al.*, 2014) and hence the negative jumps during solar maximum are consistent with the earlier reports.

5. Summary and Conclusion

Using the synoptic magnetogram data observed using NSO/KP and NSO/SOLIS instruments during the period from 1975 to April 2018, we inspected the average magnetic fields (at the photosphere) over different latitude ranges in both northern and southern hemispheres. We have noticed that not only the polar magnetic field, but the equatorial, mid-latitude, and fields in Region A are also declining, since the mid-1990s (see Figures 3, 4; and Table 1). Further, we have inspected the magnetograms extrapolated (using the PFSS method) to the heliocentric distances to 2.5 and 10 $R_{\odot}$ and they also show the same trend. We found that, during the period from the mid-1990s to April 2018, the magnetic field over different latitudes (at photosphere and inner solar-wind) declined by 11.3 – 22.2%. Using the data observed from ISEE, Japan, we inspected the normalized scintillation index [m] during 1983 – 2017. We found that the quantity m has decreased by 23.6% since the mid-1990s. From Figure 5, it is clear that the peak sunspot number from Solar Cycle 21 (in the year 1980) to Solar Cycle 24 (in the year 2014) has declined by $\approx$ 50%. Therefore, these results show a strong relationship between the global magnetic fields and the various turbulence properties in the solar wind. Also, we found that the magnetic field at relatively low heights shows a monotonic decrease (by 15.9 – 19.1%; see Table 1) and a variation of the magnetic field (due to sunspots) over each solar cycle by 5 – 10%. Such oscillating behavior disappears in the inner solar wind (*i.e.* at 2.5 and 10 $R_{\odot}$) and a clear monotonic decline of the magnetic field is seen (by 11.3 – 22.2%). In this article we show that the global coronal magnetic field of the Sun (and not just the polar fields) has monotonically decreased since (approximately) 1995. These results are significant, as many authors are predicting that we are tending towards the another "Maunder"-like minimum (Janardhan *et al.*, 2011, 2015, 2018; Pesnell and Schatten, 2018). It would be interesting to further examine the relationship between the global (large-scale) magnetic field and the properties of density turbulence (which are measured by IPS). For example, the way magnetic field and the turbulence properties in the solar wind (*i.e.* amplitude of the turbulence, density, velocity and magnetic-field fluctuations, dissipation scales, and heating rates *etc.*) are related (Bisoi *et al.*, 2014; Sasikumar Raja *et al.*, 2016, 2017, 2019). The recently launched *Parker Solar Probe* may provide valuable insights in understanding the relationship between the magnetic field and the turbulent parameters (Fox *et al.*, 2016).

Acknowledgments K.S. Raja acknowledges Marc L. De Rosa for his valuable suggestions related to the PFSS extrapolation technique. K.S. Raja acknowledges the financial support from Centre National d'études Spatiales (CNES), France. This work utilizes SOLIS data obtained by the *NSO Integrated Synoptic Program* (NISP), managed by the National Solar Observatory, which is operated by the Association of Universities for Research in Astronomy (AURA), Inc. under a cooperative agreement with the National Science Foundation. Data storage supported by the University of Colorado Boulder "PetaLibrary." Sunspot data from the World Data Center SILSO, Royal Observatory of Belgium, Brussels. The authors would like to thank the anonymous reviewer for their constructive suggestions and comments, which helped in improving the manuscript.

Disclosure of Potential Conflicts of Interest The authors declare that they have no conflicts of interest.

References

Altschuler, M.D., Newkirk, G.: 1969, Magnetic fields and the structure of the solar corona. I: Methods of calculating coronal fields. *Solar Phys.* **9**, 131. DOI. ADS.

Ananthakrishnan, S., Coles, W.A., Kaufman, J.J.: 1980, Microturbulence in solar wind streams. *J. Geophys. Res.* **85**, 6025. DOI. ADS.

Arnaud, J., Newkirk, G. Jr.: 1987, Mean properties of the polarization of the Fe XIII 10747 A coronal emission line. *Astron. Astrophys.* **178**, 263. ADS.

Asai, K., Kojima, M., Tokumaru, M., Yokobe, A., Jackson, B.V., Hick, P.L., Manoharan, P.K.: 1998, Heliospheric tomography using interplanetary scintillation observations. III – Correlation between speed and electron density fluctuations in the solar wind. *J. Geophys. Res.* **103**, 1991. DOI. ADS.

Bird, M.K.: 1981, Coronal sounding with pulsars. In: Rosenbauer, H. (ed.) *Solar Wind 4*, Max-Planck-Institute für Aeronomie, Lindau, 78. ADS.

Bird, M.K.: 1982, Coronal investigations with occulted spacecraft signals. *Space Sci. Rev.* **33**, 99. DOI. ADS.

Bisoi, S.K., Janardhan, P., Ingale, M., Subramanian, P., Ananthakrishnan, S., Tokumaru, M., Fujiki, K.: 2014, A study of density modulation index in the inner heliospheric solar wind during solar cycle 23. *Astrophys. J.* **795**, 69. DOI. ADS.

Celnikier, L.M., Muschietti, L., Goldman, M.V.: 1987, Aspects of interplanetary plasma turbulence. *Astron. Astrophys.* **181**(1), 138. ADS.

Clette, F., Svalgaard, L., Vaquero, J.M., Cliver, E.W.: 2015, In: Balogh, A., Hudson, H., Petrovay, K., von Steiger, R. (eds.) *Revisiting the Sunspot Number*, *ISSI Space Science Ser.*, Springer, New York, 35. DOI. ADS.

Fox, N.J., Velli, M.C., Bale, S.D., Decker, R., Driesman, A., Howard, R.A., Kasper, J.C., Kinnison, J., Kusterer, M., Lario, D., Lockwood, M.K., McComas, D.J., Raouafi, N.E., Szabo, A.: 2016, The solar probe plus mission: Humanity's first visit to our star. *Space Sci. Rev.* **204**, 7. DOI. ADS.

Freeland, S.L., Handy, B.N.: 1998, Data analysis with the SolarSoft system. *Solar Phys.* **182**, 497. DOI. ADS.

Hale, G.E.: 1908, On the probable existence of a magnetic field in Sun-spots. *Astrophys. J.* **28**, 315. DOI. ADS.

Harvey, J.W.: 1969, Magnetic fields associated with solar active-region prominences. Ph.D. thesis, Univ. Colorado, Boulder. ADS.

Hewish, A., Scott, P.F., Wills, D.: 1964, Interplanetary scintillation of small diameter radio sources. *Nature* **203**, 1214. DOI. ADS.

Hoeksema, J.T.: 1984, Structure and evolution of the large scale solar and heliospheric magnetic fields. Ph.D. thesis, Stanford Univ., CA. sun.stanford.edu/~todd/Hoeksema1984.pdf. ADS.

Janardhan, P., Alurkar, S.K.: 1993, Angular source size measurements and interstellar scattering at 103 MHz using interplanetary scintillation. *Astron. Astrophys.* **269**, 119. ADS.

Janardhan, P., Bisoi, S.K., Gosain, S.: 2010, Solar polar fields during cycles 21 – 23: Correlation with meridional flows. *Solar Phys.* **267**, 267. DOI. ADS.

Janardhan, P., Balasubramanian, V., Ananthakrishnan, S., Dryer, M., Bhatnagar, A., McIntosh, P.S.: 1996, Travelling interplanetary disturbances detected using interplanetary scintillation at 327 MHz. *Solar Phys.* **166**, 379. DOI. ADS.

Janardhan, P., Bisoi, S.K., Ananthakrishnan, S., Tokumaru, M., Fujiki, K.: 2011, The prelude to the deep minimum between solar cycles 23 and 24: Interplanetary scintillation signatures in the inner heliosphere. *Geophys. Res. Lett.* **38**, L20108. DOI. ADS.

Janardhan, P., Bisoi, S.K., Ananthakrishnan, S., Tokumaru, M., Fujiki, K., Jose, L., Sridharan, R.: 2015, A 20 year decline in solar photospheric magnetic fields: Inner-heliospheric signatures and possible implications. *J. Geophys. Res.* **120**, 5306. DOI. ADS.

Janardhan, P., Fujiki, K., Ingale, M., Bisoi, S.K., Rout, D.: 2018, Solar cycle 24: An unusual polar field reversal. *Astron. Astrophys.* **618**, A148. DOI. ADS.

Kojima, M., Kakinuma, T.: 1990, Solar cycle dependence of global distribution of solar wind speed. *Space Sci. Rev.* **53**(3 – 4), 173. DOI. ADS.

Lin, H., Penn, M.J., Tomczyk, S.: 2000, A new precise measurement of the coronal magnetic field strength. *Astrophys. J. Lett.* **541**, L83. DOI. ADS.

Lopez, R.E., Freeman, J.W.: 1986, Solar wind proton temperature–velocity relationship. *J. Geophys. Res.* **91**(A2), 1701. DOI. ADS.

Mackay, D.H., van Ballegooijen, A.A.: 2006, Models of the large-scale corona. I. Formation, evolution, and liftoff of magnetic flux ropes. *Astrophys. J.* **641**, 577. DOI. ADS.

Manoharan, P.K.: 2010, Ooty interplanetary scintillation – Remote-sensing observations and analysis of coronal mass ejections in the heliosphere. *Solar Phys.* **265**, 137. DOI. ADS.

Marians, M.: 1975, Computed scintillation spectra for strong turbulence. *Radio Sci.* **10**, 115. DOI. ADS.

McComas, D.J., Barraclough, B.L., Funsten, H.O., Gosling, J.T., Santiago-Muñoz, E., Skoug, R.M., Goldstein, B.E., Neugebauer, M., Riley, P., Balogh, A.: 2000, Solar wind observations over Ulysses' first full polar orbit. *J. Geophys. Res.* **105**(A5), 10419. DOI. ADS.

Mickey, D.L.: 1973, Polarization measurements in the green coronal line. *Astrophys. J. Lett.* **181**, L19. DOI. ADS.

Pesnell, W.D., Schatten, K.H.: 2018, An early prediction of the amplitude of solar cycle 25. *Solar Phys.* **293**, 112. DOI. ADS.

Querfeld, C.W., Smartt, R.N.: 1984, Comparison of coronal emission-line structure and polarization. *Solar Phys.* **91**, 299. DOI. ADS.

Ramesh, R., Kathiravan, C., Sastry, C.V.: 2010, Estimation of magnetic field in the solar coronal streamers through low frequency radio observations. *Astrophys. J.* **711**, 1029. DOI. ADS.

Sasikumar Raja, K., Ramesh, R.: 2013, Low-frequency observations of transient quasi-periodic radio emission from the solar atmosphere. *Astrophys. J.* **775**, 38. DOI. ADS.

Sasikumar Raja, K., Ramesh, R., Hariharan, K., Kathiravan, C., Wang, T.J.: 2014, An estimate of the magnetic field strength associated with a solar coronal mass ejection from low frequency radio observations. *Astrophys. J.* **796**, 56. DOI. ADS.

Sasikumar Raja, K., Ingale, M., Ramesh, R., Subramanian, P., Manoharan, P.K., Janardhan, P.: 2016, Amplitude of solar wind density turbulence from 10 to 45 $R_{\odot}$. *J. Geophys. Res.* **121**, 11. DOI. ADS.

Sasikumar Raja, K., Subramanian, P., Ramesh, R., Vourlidas, A., Ingale, M.: 2017, Turbulent density fluctuations and proton heating rate in the solar wind from 9-20 $R_{\odot}$. *Astrophys. J.* **850**, 129. DOI. ADS.

Sasikumar Raja, K., Subramanian, P., Ingale, M., Ramesh, R.: 2019, Dissipation scale lengths of solar wind turbulence. *Astrophys. J.* **872**, 77. DOI. ADS.

Sastry, C.V.: 2009, Polarization of the thermal radio emission from outer solar corona. *Astrophys. J.* **697**, 1934. DOI. ADS.

Schatten, K.H., Wilcox, J.M., Ness, N.F.: 1969, A model of interplanetary and coronal magnetic fields. *Solar Phys.* **6**, 442. DOI. ADS.

Schrijver, C.J., De Rosa, M.L.: 2003, Photospheric and heliospheric magnetic fields. *Solar Phys.* **212**, 165. DOI. ADS.

Schrijver, C.J., Title, A.M.: 2003, The magnetic connection between the solar photosphere and the corona. *Astrophys. J. Lett.* **597**, L165. DOI. ADS.

Stelzried, C.T., Levy, G.S., Sato, T., Rusch, W.V.T., Ohlson, J.E., Schatten, K.H., Wilcox, J.M.: 1970, The quasi-stationary coronal magnetic field and electron density as determined from a Faraday rotation experiment. *Solar Phys.* **14**, 440. DOI. ADS.

Tokumaru, M., Kojima, M., Fujiki, K.: 2010, Solar cycle evolution of the solar wind speed distribution from 1985 to 2008. *J. Geophys. Res.* **115**, A04102. DOI. ADS.

van Ballegooijen, A.A., Priest, E.R., Mackay, D.H.: 2000, Mean field model for the formation of filament channels on the Sun. *Astrophys. J.* **539**, 983. DOI. ADS.

Venugopal, V.R., Ananthakrishnan, S., Swarup, G., Pynzar, A.V., Udaltsov, V.A.: 1985, Structure of PKS 1148-001. *Mon. Not. Roy. Astron. Soc.* **215**, 685. DOI. ADS.

Wang, Y.-M., Sheeley, N.R. Jr.: 1992, On potential field models of the solar corona. *Astrophys. J.* **392**, 310. DOI. ADS.

Zhao, X., Hoeksema, J.T.: 1995, Prediction of the interplanetary magnetic field strength. *J. Geophys. Res.* **100**, 19. DOI. ADS.